PHYSICAL REVIEW D **86,** 103536 (2012)

Antideuterons from dark matter annihilations and hadronization model dependence

L. A. Dal[1] and M. Kachelrieß[2]
[1]*Department of Physics, University of Oslo, Oslo, Norway*
[2]*Department of Physics, NTNU, Trondheim, Norway*
(Received 24 July 2012; published 27 November 2012)

We calculate the antideuteron yield in dark matter annihilations on an event-by-event basis using the HERWIG++ Monte Carlo generator. We present the resulting antideuteron fluxes for quark and gauge boson final states. As deuteron production in the coalescence model depends on momentum differences between nucleons that are small compared to $\Lambda_{\rm QCD}$, it is potentially very sensitive to the hadronization model employed. We therefore compare our antideuteron yields to earlier results based on PYTHIA, thereby estimating their uncertainties. We also briefly discuss the importance of $n > 2$ final states for annihilations of heavy dark matter particles.

DOI: 10.1103/PhysRevD.86.103536 PACS numbers: 95.35.+d, 27.10.+h

I. INTRODUCTION

Despite various cosmological and astrophysical indications for the presence of nonbaryonic dark matter (DM), its particle nature has yet to be proven. Restricting the space of candidates to thermal relics, the thermally averaged annihilation cross section $\langle\sigma v\rangle$ at freeze-out is fixed by the DM abundance, while the DM mass $M_{\rm DM}$ is only weakly constrained: Unitarity of the S matrix constrains the mass of any thermal relic as $m \lesssim 50$ TeV [1], while the requirement that the DM is cold translates for thermal relics into a lower mass limit of the order 10 keV.

One strategy towards DM detection is to search for its self-annihilation (or decay) products. The annihilation of symmetric DM leads to equal injection rates of matter and antimatter particles into the Galaxy, while the cosmic ray flux from astrophysical sources is matter-dominated. A possible way to detect DM is therefore to carefully estimate the expected antimatter fluxes from astrophysical sources, and then to search for any excess. The authors of Ref. [2] suggested antideuterons as a signature in addition to the usually discussed antiproton and positron signal from DM annihilations. In particular, they argued that the DM antideuteron spectra are much flatter at low energies than those from cosmic-ray–gas interactions.

The correct application of the coalescence model in deuteron production requires its implementation on an event-by-event basis [3,4]. Since deuteron production depends on momentum differences p_0 that are small or comparable to $\Lambda_{\rm QCD} \sim 200$ MeV, one may expect a rather strong dependence of the results on the hadronization models employed in the Monte Carlo simulation. Moreover, the coalescence model probes not only the energy spectrum of nucleons, but also their two-particle correlations in momentum space. Since the physics underlying different hadronization models—e.g., cluster hadronization versus string fragmentation—varies strongly, the choice of hadronization model could thus have a profound effect on the generated antideuteron spectra.

The main aim of this work is therefore to derive results for the antideuteron yields calculated using the HERWIG++ [5] version 2.4.2 (based on a cluster hadronization model) and to compare them to earlier results using PYTHIA [6] (based on string fragmentation). We also briefly discuss the importance of $n > 2$ final states for annihilations of heavy DM particles.

II. DEUTERON PRODUCTION AND HADRONIZATION

The fusion of (anti)protons and (anti)neutrons into (anti) deuterons is usually described with the so-called coalescence model. This model is based on the assumption that any nucleons with a momentum difference $\Delta p < p_0$ for some given p_0 will merge and form a nucleus. In its initial form, the model was applied to deuteron production in nucleus-nucleus interactions. In the simplest approximation, the final-state hadrons in nucleus-nucleus scattering are formed in a ''fireball'' and are emitted close to isotropically in the center-of-mass (c.m.) frame. Assuming additionally that correlations between nucleons are negligible, the antideuteron energy spectra in the lab frame can be derived from the energy spectra of nucleons as [7,8]

$$\frac{dN_{\bar d}}{dT_{\bar d}} = \frac{p_0^3}{6}\,\frac{m_{\bar d}}{m_{\bar n} m_{\bar p}}\,\frac{1}{\sqrt{T_{\bar d}^2 + 2 m_{\bar d} T_{\bar d}}}\,\frac{dN_{\bar n}}{dT_{\bar n}}\,\frac{dN_{\bar p}}{dT_{\bar p}}. \qquad (1)$$

Here, p_0 is the maximal momentum difference allowed within a $\bar p\,\bar n$ pair in order to form an antideuteron according the coalescence model, m_d, m_p, and m_n denote the deuteron, proton, and neutron masses, respectively, and the nucleon spectra on the right-hand side are to be evaluated at the value $T_{\bar p} = T_{\bar n} = T_{\bar d}/2$ of the kinetic energy $T_i = E_i - m_i$.

The constant prefactor in Eq. (1) varies depending on the assumptions made in its derivation [4]. Such a factor can, however, be absorbed by redefining p_0. For later reference,

we note that our definition of p_0 agrees with the one of Ref. [3], while the one of Refs. [9,10] differs by a factor 2.

The coalescence model can easily be implemented directly in a Monte Carlo simulation by comparing the momenta of the final-state nucleons in their respective c.m. frames for each individual annihilation event. We will from now on refer to results from calculations where coalescence was applied on an event-by-event basis within the Monte Carlo as "Monte Carlo" results, while results from calculations where coalescence was applied to the average antiproton and antineutron energy spectra using Eq. (1) will be referred to as "isotropic" results. Correspondingly, we refer to the two approaches as the Monte Carlo approach and the isotropic approach.

A. Determining p_0

The momentum threshold p_0 for the formation of deuterons is found in both approaches by running simulations and adjusting p_0 such that the computational result matches the experimental one. Antideuteron production in e^+e^- collisions was studied by the ALEPH Collaboration [11] using LEP-I data. At the Z resonance, each hadronic event was found to give rise to $(5.9 \pm 1.8 \pm 0.5) \times 10^{-6}$ antideuterons in the momentum range $0.62\ \text{GeV} < k_{\bar{d}} < 1.03\ \text{GeV}$ in the angular acceptance range $|\cos\vartheta| < 0.95$ of the detector.

Our simulations using HERWIG++ reproduce the experimentally measured antideuteron yield choosing $p_0 = 110$ MeV in the Monte Carlo approach and $p_0 = 126$ MeV in the isotropic approach, respectively. Note that the p_0 values differ in general for the two methods, and should therefore be self-consistently calibrated.

There is a significant range in the value of p_0 used in the literature. Reference [9] suggests a window between 66 MeV and 105 MeV for the isotropic approach (note that their definition of p_0 requires a rescaling of p_0 by 2 to compare with our values), while Kadastik *et al.* [3] use a value of $p_0 = 160$ MeV for both the isotropic and Monte Carlo approach.

The relatively large difference of 45% between the p_0 values found by us using HERWIG++ and Kadastik *et al.* using PYTHIA indicates that the differing hadronization models do indeed lead to physically different predictions. Since the momentum range used for the calibration is very small, our normalization procedure does not even guarantee that the total number of antideuterons predicted by HERWIG++ and PYTHIA for our reference process $e^+e^- \to Z^0 \to$ hadrons agrees. In order to illustrate this point, we repeated the calibration using PYTHIA (version 8.160). In Fig. 1, we compare the energy spectrum TdN/dT of antideuterons calculated by us with the two QCD simulations. By construction, the two spectra cross in the calibration range, but PYTHIA predicts a harder energy spectrum and a total yield of antideuterons larger by a factor 2 than HERWIG. Going to higher c.m. energies or DM masses, one expects moreover that the spectral shape and the total number of antideuterons evolves differently in the two hadronization schemes.

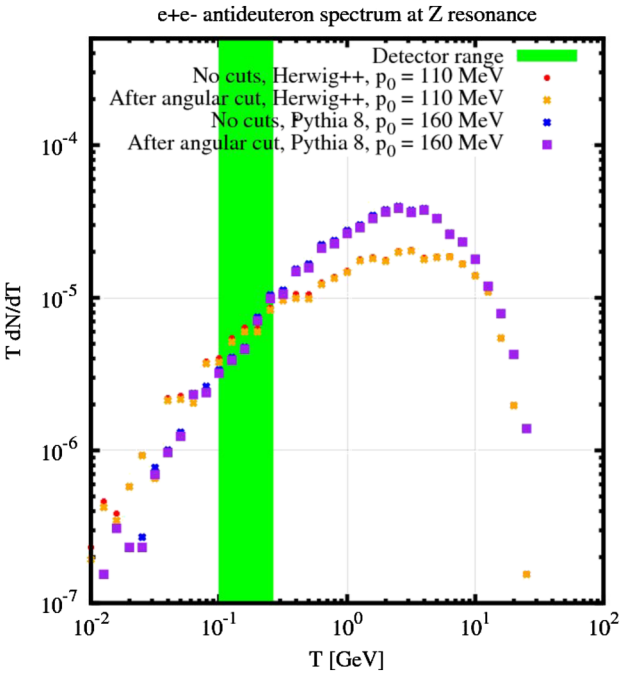

FIG. 1 (color online). Comparison of the energy spectrum TdN/dT of antideuterons for the calibration reaction, with and without the angular cut $|\cos\vartheta| < 0.95$. The energy range used for the calibration is shown as the green area.

Note that the single nucleon spectra calculated with HERWIG++ and PYTHIA agree quite well, implying that the large differences found in the antideuteron yield are caused by differences in the two-particle correlations of the $\bar{p}\,\bar{n}$ pairs.

B. The hadronization models

Let us recall briefly the main features of the hadronization models employed in HERWIG++ and PYTHIA: The latter implements the string fragmentation or Lund model which is based on a linear confinement picture [12]. As supported by lattice QCD studies, this model assumes that the energy stored in the color dipole field between a color charge and an anticharge increases linearly with their separation. As the $q\bar{q}$ pair moves apart from their common production vertex, a color flux tube is stretched between them which is described by a massless relativistic string with no transverse degrees of freedom. The potential energy stored in the string increases as the quarks separate until the string breaks producing a new color-singlet $q'\bar{q}'$ pair. The string breakup is modeled as a tunneling process, leading to a flavor-independent Gaussian spectrum for the transverse momentum p_T. Baryon production in the Lund model is described similarly as a tunneling process.

While the Lund model used in PYTHIA is based on a linear confinement picture, the cluster fragmentation

model of HERWIG++ assumes "preconfinement" and local parton-hadron duality [13]. At the end of the perturbative QCD cascade, gluons are split nonperturbatively into light quark-antiquark or diquark-antidiquark pairs. Color connected quarks are then combined to form color singlet clusters, using prescribed mass distributions which fall rapidly for large masses. If a cluster is too light to decay, it is replaced by the lightest hadron of its flavor, and its mass is shifted to the correct value by exchanging momentum with a neighboring cluster. Heavier clusters fragment according to empirical prescriptions. For an extensive discussion of the physics underlying these QCD Monte Carlo simulations we recommend interested readers to consult Refs. [12,14].

C. Uncertainty from the model parameters

While our main focus is the difference in the antideuteron spectrum between the two hadronization models, we also investigate the inherent uncertainty of the HERWIG++ cluster hadronization. This uncertainty emerges because ranges of values for the hadronization parameters are compatible with experimental data. We choose the hadronization parameters and ranges studied in Ref. [15], as shown in Table I. We run simulations using the "high" or "low" value for a single parameter, while keeping the other parameters at their default value. All simulations were done for the previously discussed case of antideuteron production at the Z resonance using 10^8 events and $p_0 = 110$ MeV. We then calculate the ratios

$$R_P \equiv \frac{dN/dT|_{\text{modified}}}{dN/dT|_{\text{default}}},$$

of the antideuteron spectra obtained using modified parameters with respect to the spectra obtained using default values. In order to distinguish between changes due to modified two-particle correlations and trivial changes due to modified antinucleon multiplicities, we additionally consider the corresponding ratio for antideuteron spectra calculated using Eq. (1) in the isotropic coalescence approach. Parameters that affect the two-particle correlations are of particular interest, as they could give significant changes in the antideuteron spectrum while keeping the antiproton spectrum in agreement with observed values. We note that the value of p_0 should be adjusted according to the antideuteron yield. For cases where the ratio is largely independent of energy, this recalibration can significantly reduce or entirely absorb the effect of adjusting the parameter.

TABLE I. Varied parameters of HERWIG++ with the corresponding "low," default, and "high" values and the resulting ratios $R_{P,\text{tot}}$ of total antideuteron multiplicities obtained in the event-by-event Monte Carlo approach.

Parameter	"Low"	$R^{\text{low}}_{P,\text{tot}}$	Default	"High"	$R^{\text{high}}_{P,\text{tot}}$
GLUONMASS	0.75	0.85	0.95	1.00	0.81
ALPHAMZ	0.10	1.62	0.12	0.12	1.00
CLPOWLIGHT	0.50	0.36	1.28	4.00	0.93
CLMAXLIGHT	3.00	0.97	3.25	4.20	0.84
CLSMRLIGHT	0.30	1.04	0.78	3.00	0.96
PSPLITLIGHT	1.00	0.81	1.14	2.00	2.49
PWTDIQUARK	0.10	0.08	0.49	0.50	1.00
PWTSQUARK	0.50	0.99	0.68	0.80	1.01

In Fig. 2, we show the ratios obtained varying the parameter PSPLITLIGHT as an example of a case where the antideuteron yield changes nontrivially. While the ratio as a function of energy has a shape similar to that which can be expected from the changes in the antinucleon spectra, the change in the overall yield is significantly larger. The parameter CLPOWLIGHT is another case where the antideuteron yield changes nontrivially. As seen in Fig. 3, this is, however, a case where also the shape of the spectrum deviates significantly from what can be expected from the changes in the antinucleon spectra. We find a similar behavior for the parameter ALPHAMZ, but in this case the nontrivial component is smaller and the ratios are flatter. As an example of a parameter that influences the antideuteron yield only via the antinucleon multiplicity, we show the ratios obtained from varying PWTDIQUARK in Fig. 4. For this and the remaining parameters, the ratio R_P is a rather flat function of energy, and is well represented by the ratio $R_{P,\text{tot}}$ of the total antideuteron multiplicities, as given in Table I.

Overall, we found no case where a change in a parameter of the cluster fragmentation model strongly influenced the antideuteron spectra without also leading to a significant change in the nucleon spectra. Moreover, a recalibration of p_0 will in most cases contribute to reduce changes in the antideuteron spectrum from adjustments of hadronization

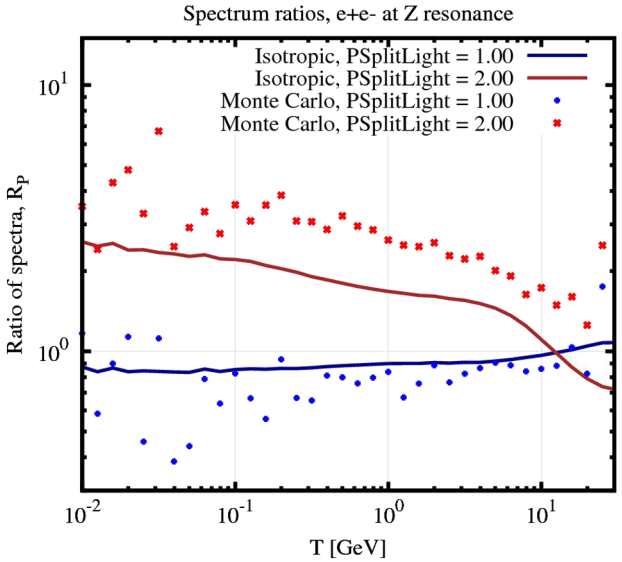

FIG. 2 (color online). Ratio R_P for antideuteron spectra at the Z resonance, varying the parameter PSPLITLIGHT.

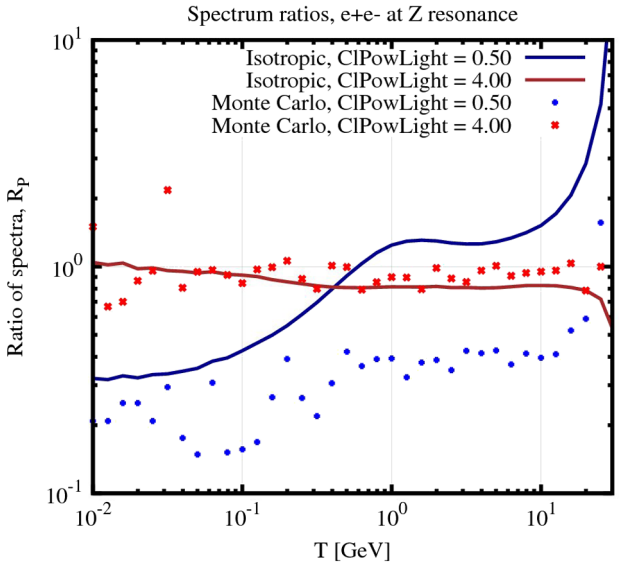

FIG. 3 (color online). Ratio R_P for antideuteron spectra at the Z resonance, varying the parameter CLPOWLIGHT.

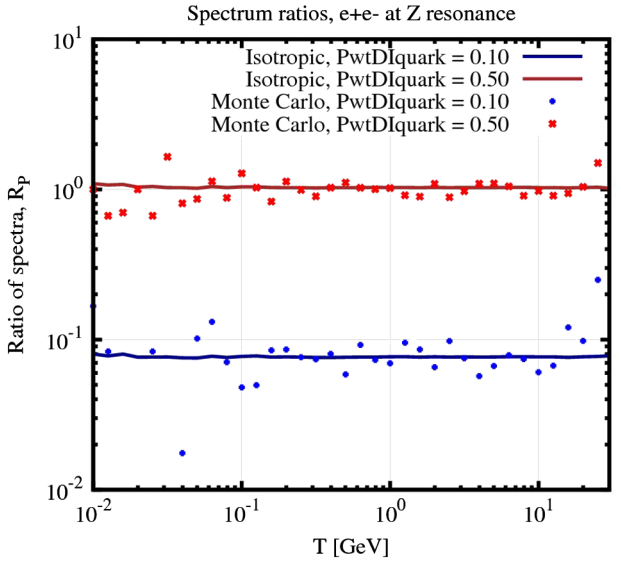

FIG. 4 (color online). Ratio R_P for antideuteron spectra at the Z resonance, varying the parameter PWTDIQUARK.

parameters. We therefore conclude that the uncertainties within the hadronization model used by HERWIG++ does not lead to a spread in the predicted antideuteron yield that is significantly larger than the factor of a few difference between HERWIG++ and PYTHIA.

III. DM ANTIDEUTERON SPECTRA

Our results were generated using 10^8 events for each annihilation channel and dark matter mass, and are generally presented in terms of the scaled kinetic energy $x \equiv T/M_{\rm DM}$, where $M_{\rm DM}$ is the dark matter mass. For practical reasons, we used the lightest neutralino in the minimal supersymmetric standard model as a DM particle, thus allowing us to use MadGraph [16] to generate events to be fed into HERWIG++ for showering and hadronization. Note that while the branching ratios into different final states are strongly model-dependent, the energy spectrum of a specific final state is—except in cases where spin correlations are important—mainly determined by the c.m. energy $\sqrt{s} = 2M_{\rm DM}$.

A. The antideuteron fragmentation spectra

The antideuteron fluxes from the isotropic and Monte Carlo approaches obtained by us using HERWIG++ are plotted for DM masses of 300 GeV and 1 TeV in Fig. 5. In the $b\bar{b}$ case, the low-x part of the energy spectra dN/dx is roughly the same for the two methods. The spectra in the Monte Carlo approach extend, however, towards much larger x. For the W^+W^- case, there is a significant difference in the antideuteron spectrum for all x between the two approaches. For 1 TeV, the difference is of order 100 at low x, while it is around a factor ~30 for 300 GeV. The shapes of the spectra also differ somewhat between the two approaches, with the maxima of xdN/dx shifted towards higher x in the Monte Carlo approach.

It is clear that when using the correct Monte Carlo approach, the difference in magnitude between the $b\bar{b}$ and W^+W^- antideuteron spectra becomes much smaller than in the isotropic approach. Another interesting feature is that this difference appears to depend on the DM mass.

In order to investigate the dependence of the antideuteron spectra on the DM mass, we plot the total number of antideuterons produced against the DM mass for the two approaches in Fig. 6. Comparing this graph to the corresponding one of Ref. [3] obtained using PYTHIA, we find the general behavior of the antideuteron yield as function of channel and approach agrees well. Comparing individual energy spectra, we observe a sharper drop at high energies in the spectra produced by HERWIG++. We also note some differences in the overall magnitudes, and we therefore proceed by comparing our HERWIG++ results to those of Kadastik *et al.* [3] in more detail. For their results we use the data files (without electroweak corrections) from Ref. [17], which were generated using PYTHIA version 8.135.

In Fig. 7, we show the ratio

$$R \equiv \frac{dN/dx|_{\rm HERWIG++}}{dN/dx|_{\rm PYTHIA}},$$

of the antideuteron energy spectra calculated with HERWIG++ and PYTHIA, respectively. In the peak region, this ratio is close to 0.5 for the W^+W^- channel, while it is close to 0.3 for the $b\bar{b}$ channel. In the forward region $x \to 1$, PYTHIA predicts a significantly higher antideuteron yield than HERWIG++, leading to a drop of the ratio R. As expected from the calibration reaction (cf. Fig. 1), the ratio

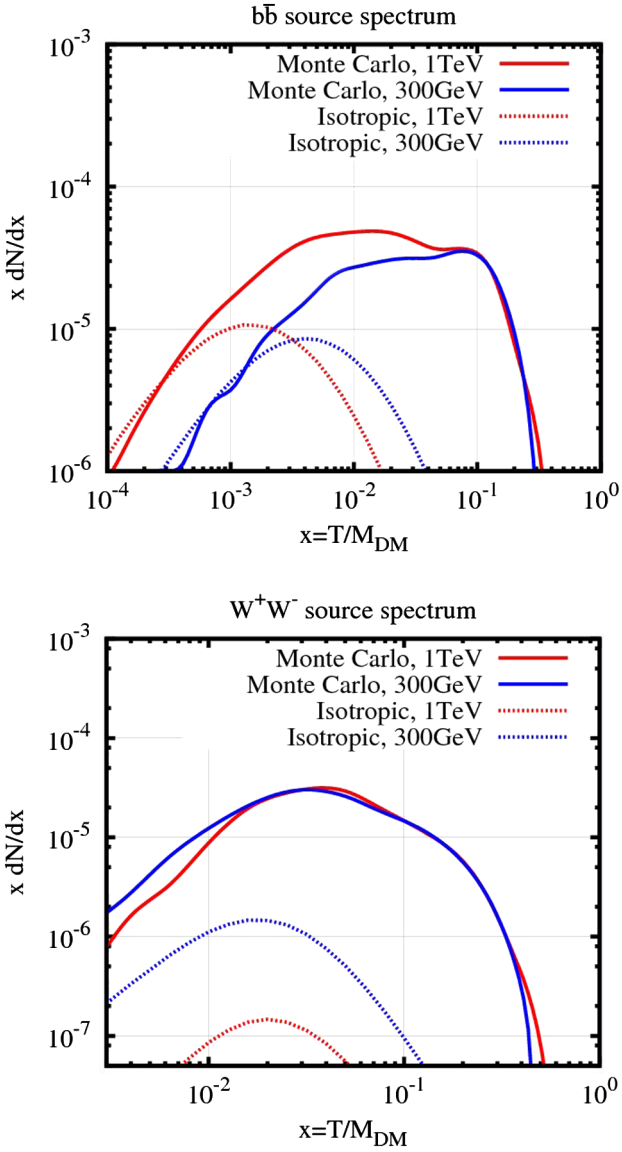

FIG. 5 (color online). Antideuteron source spectra for dark matter annihilations into $b\bar{b}$ (top) and W^+W^- (bottom). The solid lines show the spectra for per-event coalescence within the Monte Carlo, while the dotted lines show the spectra for coalescence of the average antiproton and antineutron spectra. Red lines show the result for a dark matter mass of 1 TeV; blue lines for 300 GeV.

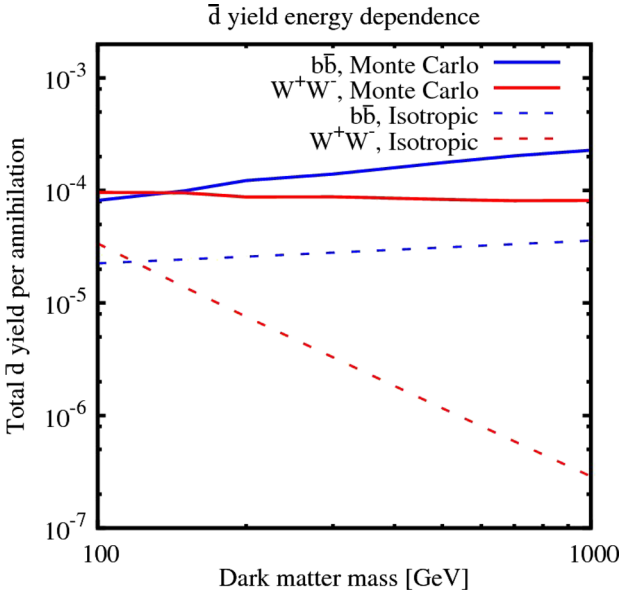

FIG. 6 (color online). Average total antideuteron yield per DM annihilation event. The solid lines show the results using per-event coalescence, while the dashed lines show the results using the isotropic approximation.

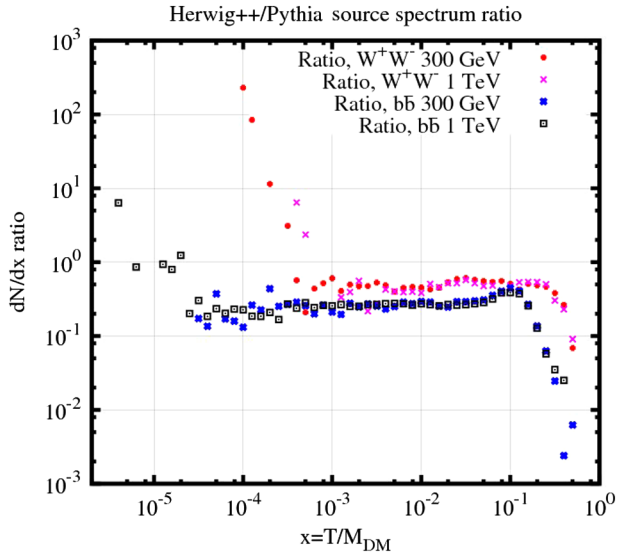

FIG. 7 (color online). Ratio R of the antideuteron spectra predicted by HERWIG++ and PYTHIA as function of x for neutralino annihilations with mass 300 GeV and 1 TeV, respectively.

R lies below one in the peak region, followed by a crossover to $R > 1$ at lower x. The expected crossover is not seen in the 300 GeV quark case, possibly due to insufficient statistics at low x. For the gauge bosons, the x value for which the ratio crosses one appears to be shifted slightly toward higher values with increasing DM mass, but the uncertainty with 10^8 events is too large to determine the crossover points precisely. For the quark case, the crossing region is shifted towards lower x. In order to see if there is a DM mass dependence of the crossing point in the quark channel, we also investigate the ratio at $M_{\rm DM} = 50$ GeV, as seen in Fig. 8. In addition to the b quarks studied in the rest of the article, the figure also includes the corresponding ratio for annihilations into light quarks (u, d, s). We see that not only does the crossover for the b-quark case appear at higher x for lower $M_{\rm DM}$, but the ratios of the antideuteron energy spectra in general also differ somewhat between light and heavy quarks.

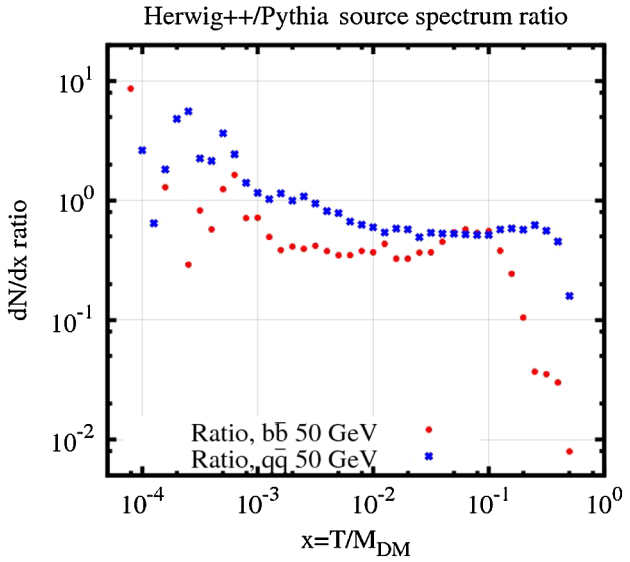

FIG. 8 (color online). Ratio R of the antideuteron spectra predicted by HERWIG++ and PYTHIA as function of x for $\chi\chi \to b\bar{b}$ and $\chi\chi \to q\bar{q}$ with $m_\chi = 50$ GeV and $q = u, d, s$.

B. Interpretation

The perhaps most striking feature of Fig. 6 is how strongly the impact of going from the isotropic to the Monte Carlo approach varies between the $b\bar{b}$ and W^+W^- channel. In the latter case, changing the DM mass by a factor 10 leads to a factor 100 difference in the antideuteron yield predicted by the two approaches, while in the former case the prediction differs only by a factor 3. This suggests that the basic assumption underlying the isotropic approach, namely an uncorrelated isotropic emission of the final-state particles, is not too strongly violated for $q\bar{q}$ final states.

To illustrate this effect, we show in Fig. 9 the distribution of the angles between the momenta of antiproton and antineutron pairs. These distributions are strongly peaked for angles near 0 and π for the W^+W^- channel, while the peaks are much less pronounced for $b\bar{b}$. More importantly, in the quark channel the shape of the distribution changes only mildly when increasing the DM mass, while the peaks in the W^+W^- channel increase strongly.

The latter effect is a simple reflection of relativistic beaming: The W's fed into HERWIG++ from MadGraph are decaying on shell, and their decay product is emitted in a cone of opening angle $\vartheta \sim m_W/M_{\rm DM}$. The relativistic beaming in itself does not affect coalescence in the Monte Carlo approach, as the nucleon momenta are to be evaluated in the c.m. frame of the respective $\bar{p}\,\bar{n}$ pairs. The fact that the bosons are decaying on shell, however, implies that the nucleon multiplicity—and thus the antideuteron multiplicity—remains constant with increasing $M_{\rm DM}$, as shown in Fig. 10. Using the (wrong) Eq. (1) derived in the isotropic approach,

$$\frac{dN_{\bar{d}}}{dx} \propto \frac{1}{M_{\rm DM}^2} \frac{dN_{\bar{n}}}{dx} \frac{dN_{\bar{p}}}{dx}, \tag{2}$$

one would instead expect a $1/M_{\rm DM}^2$ suppression in the antideuteron yield, as is reflected by the isotropic W^+W^- result in Fig. 6.

In contrast to the gauge bosons, the b's are treated as virtual particles and start QCD cascades. Although these cascades are angular-ordered and lead to confined jets, the overall shape of the event is not too far from spherically symmetric. Moreover, the two initial back-to-back jets are color connected, and partons from the two jets have to combine in order to produce colorless final states.

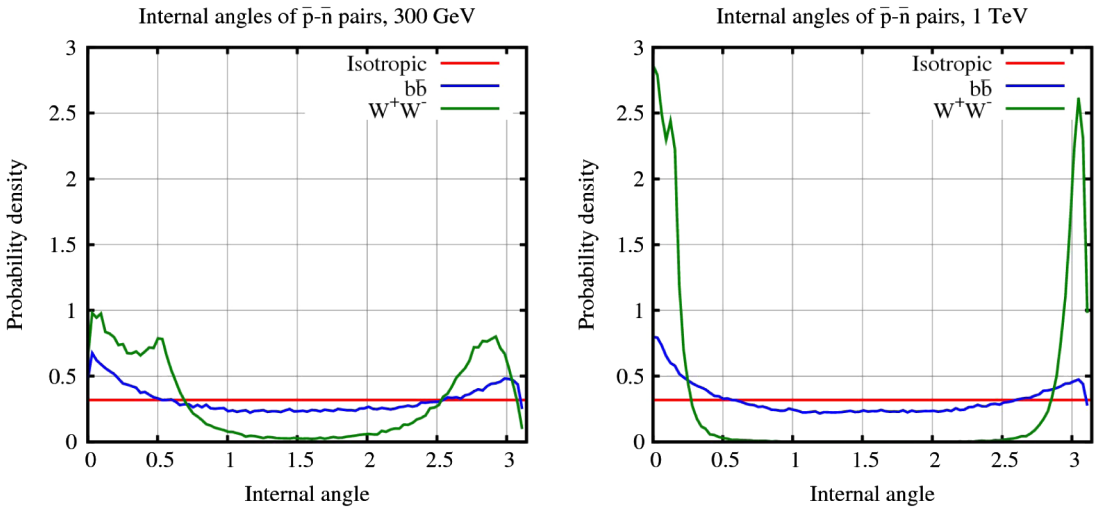

FIG. 9 (color online). Distribution of the angles between the momenta of antiprotons and antineutrons; left for $M_{\rm DM} = 300$ GeV, right for $M_{\rm DM} = 1$ TeV. Blue and green lines show the distribution in Monte Carlo approach result for $b\bar{b}$ and W^+W^-, respectively, while the red lines show the result of an isotropic distribution for comparison.

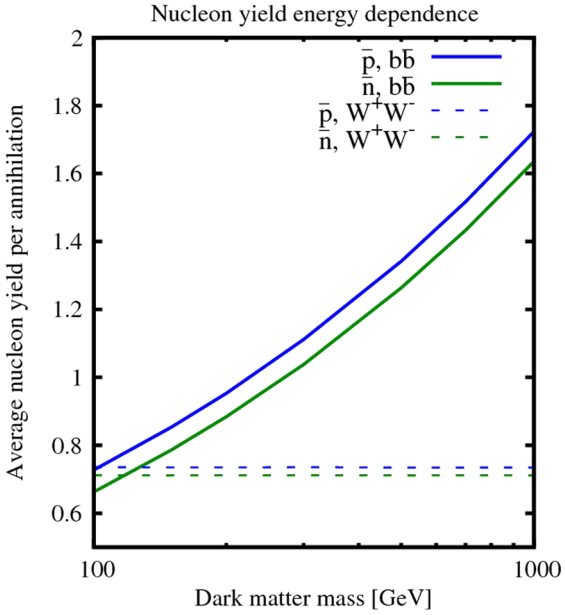

FIG. 10 (color online). Average total antiproton and antineutron yields per annihilation event as function of the dark matter mass. Lighter (green) lines indicate antineutrons, while darker (blue) lines indicate antiprotons. The solid lines show the results for the $b\bar{b}$ case, while the dashed lines show the results for the W^+W^- case.

The fact that the antideuteron yield does not show the $1/M_{\mathrm{DM}}^2$ suppression in the $b\bar{b}$ channel using the isotropic approach can also be explained. In this case, the growth of the nucleon multiplicity shown in Fig. 10 with M_{DM} overcompensates for the $1/M_{\mathrm{DM}}^2$ factor, leading to a slight increase of the antideuteron yield even in the isotropic approach.

Finally, we discuss the ratios of the HERWIG++ and PYTHIA fragmentation spectra. As already mentioned, the x for which R crosses one in the W^+W^- channel appears to shift slightly towards higher x with increasing DM mass: As the gauge bosons decay on shell, their decay products are boosted according to the DM mass, and for $M_{\mathrm{DM}} \gg m_W$ we expect $T_{\bar{d}}$ to increase linearly with M_{DM}. With the T value of the crossover point increasing linearly with M_{DM}, the corresponding $x = T/M_{\mathrm{DM}}$ should then converge towards a constant value with increasing DM masses.

In the $b\bar{b}$ channel, however, we see from Figs. 7 and 8 that the x value of the crossing region appears to decrease as $\sim 1/M_{\mathrm{DM}}$, such that the crossing occurs at a roughly constant value of the antideuteron kinetic energy $T_{\bar{d}}$. Note, however, that the drop in the ratio for $x \to 1$ appears at a constant value of x rather than T.

Using the differences between HERWIG++ and PYTHIA as an estimate for the uncertainty introduced by the hadronization models, we conclude that the high-energy part of the antideuteron spectra cannot be predicted reliably for either the gauge boson or quark channels. For the $b\bar{b}$ channel, the spectrum has an uncertainty of a factor ~ 3 from $x \sim 10^{-1}$ down to $T \sim 10^{-2}$ GeV, below which the uncertainty increases. For the gauge bosons, we find an uncertainty of ~ 2 for $10^{-3} \lesssim x \lesssim 0.5$, with rapidly increasing uncertainties outside this range. For the W^+W^- channel, the crossover point, and consequently the high uncertainty region at low energies, moves linearly towards higher T with increasing DM mass. Since T, rather than x, is the relevant quantity for the observable intensity of antideuterons, this implies that observationally relevant energies could lie in the region with large uncertainties for DM masses in the TeV range and above.

C. Higher order processes

Motivated by the PAMELA excess, previous works have discussed the annihilation and the resulting antideuteron fluxes of DM particles up to 30 TeV [3,10]. The unitarity limit of 50 TeV implies that the partial wave amplitude for the annihilation of such heavy DM particles is close to one. Thus DM particles with masses $\gtrsim 10$ TeV should behave as *strongly* interacting particles, and higher order processes should give an important contribution to their total annihilation cross section.

As a test of this conjecture, we calculated the annihilation cross sections for $\tilde{\chi}_1^0\tilde{\chi}_1^0 \to W^+W^-$, and for the higher order tree-level processes in which one and two extra Z bosons are emitted. The calculations were performed for several different neutralino masses in the range 200 GeV to 2 TeV. Using these cross sections, we calculated the branching ratios for these processes, normalized to a sum of 1. The results from these calculations are plotted in Fig. 11.

Figure 11 shows as expected that the relative contribution from higher order processes is negligible for low neutralino masses. The contributions do, however, increase rapidly with increasing masses. For 2 TeV, the branching ratio for W^+W^-Z is roughly 10% of that for the tree-level process. While the process involving two additional Z bosons is more strongly suppressed for low neutralino masses than the single Z-boson process, its relative contribution increases faster with increasing masses than for W^+W^-Z.

Extrapolating our results, we expect the contribution from higher order processes to become significant for a neutralino mass in the 10 TeV range [18]. The emission of additional Z bosons is, of course, not the only possible higher order process, and when performing calculations in the multi-TeV range, the contributions from a number of processes should be considered.

Note also that the results of this subsection are more model-dependent than the previous ones. For DM models other than the minimal supersymmetric standard model, the DM mass where final states with $n > 2$ particles become important may be lower.

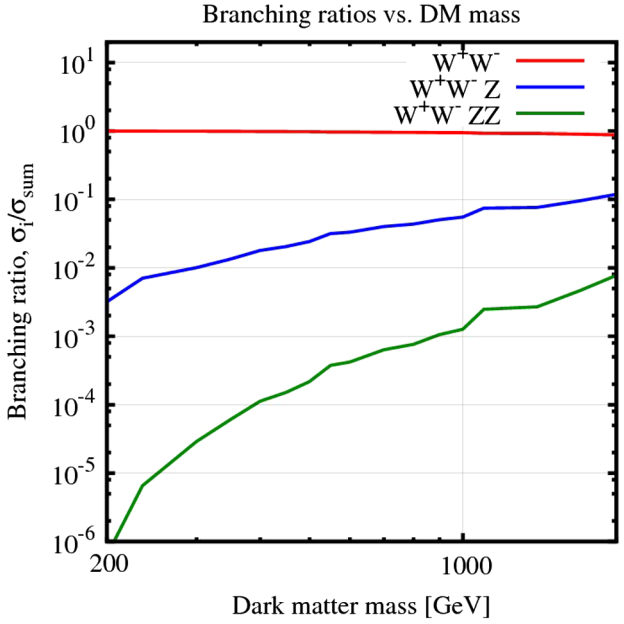

FIG. 11 (color online). Branching ratios for various annihilation channels as function of the dark matter (neutralino) mass. The red line shows the benchmark branching ratio for the tree-level process $\tilde{\chi}_1^0\tilde{\chi}_1^0 \to W^+W^-$. The blue and green lines show the branching ratios for the higher order processes $\tilde{\chi}_1^0\tilde{\chi}_1^0 \to W^+W^-Z$ and $\tilde{\chi}_1^0\tilde{\chi}_1^0 \to W^+W^-ZZ$, respectively.

IV. ANTIDEUTERON INTENSITY AT EARTH

We now move from the antideuteron spectra produced in a single annihilation to the calculation of the resulting antideuteron intensity at Earth. As charged particles scatter on fluctuations of the Galactic magnetic field with variation scales comparable to their Larmor radius, their propagation resembles a random walk and is well described by the diffusion approximation. We model this random walk using the so-called two-zone propagation model for the Galaxy. This is a cylindrical diffusion model consisting of a magnetic halo and a thin gaseous disk of radius $R = 20$ kpc and half-heights L (a free parameter) and $h = 100$ pc, respectively. For the numerical values of the parameters in this model, we adopt the three sets presented in Ref. [19] to yield maximal, median, and minimal antiproton fluxes from DM annihilations while being compatible with the observed B/C ratio. These sets are labeled "max," "med," and "min," respectively, and listed in Table II. Assuming steady state

TABLE II. Propagation parameters for the max, med, and min models.

Model	L in kpc	δ	D_0 in kpc^2 Myr^{-1}	V_c in km s^{-1}
Max	15	0.46	0.0765	5
Med	4	0.7	0.0112	12
Min	1	0.85	0.0016	13.5

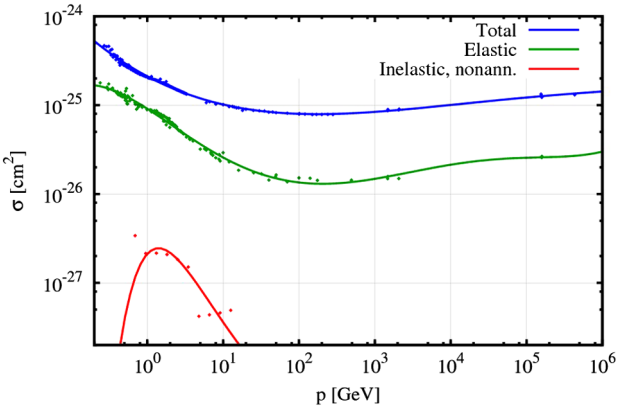

FIG. 12 (color online). Cross section data for antideuterons on interstellar protons as a function of the antideuteron momentum. The points indicate experimental data, while the lines show the fits to the data which were used in our calculations.

conditions, the diffusion equation neglecting reacceleration is given by

$$-D(T)\nabla^2 f + \frac{\partial}{\partial z}(\mathrm{sign}(z) f V_c) = Q - 2h\delta(z)\Gamma_{\mathrm{ann}}(T) f, \tag{3}$$

where $f(\mathbf{x}, T) = dN_{\bar{d}}/dT$ is the number density of antideuterons per unit kinetic energy, $D(T) = D_0\beta\mathcal{R}^\delta$ the (spatial) diffusion coefficient, V_c a convective wind perpendicular to the Galactic disk, z the vertical coordinate, $\beta = v/c$ the velocity, and $\mathcal{R}$ the rigidity of antideuterons.

The term $\Gamma_{\mathrm{ann}}(T)$ in Eq. (3) accounts for annihilations of antideuterons on the interstellar medium. The annihilation rate is given by

$$\Gamma_{\mathrm{ann}} = (n_H + 4^{\frac{2}{3}} n_{\mathrm{He}})\langle\sigma_{\bar{d}p}^{\mathrm{ann}} v\rangle, \tag{4}$$

where the factor $4^{\frac{2}{3}}$ accounts for the different cross sections of H and He interactions assuming simple geometrical scaling, and we use $n_{\mathrm{H}} \approx 1$ cm^{-3} and $n_{\mathrm{He}} \approx 0.07 n_{\mathrm{H}}$ as the number density of hydrogen and helium in the disk, respectively. The fit to the experimental data [20,21] we used for these reactions is shown in Fig. 12.

Finally, the source term Q is fixed by the DM halo profile, which we choose as either a Navarro-Frenk-White (NFW) profile [22] ($\alpha = 1$, $\beta = 3$, $\gamma = 1$) or an isothermal profile ($\alpha = 2$, $\beta = 2$, $\gamma = 0$) in

TABLE III. Density profile parameters.

DM halo profile	ρ_0 in GeV/cm^3	a in kpc
NFW	0.26	20
Isothermal	1.16	5
Einasto	0.06	20

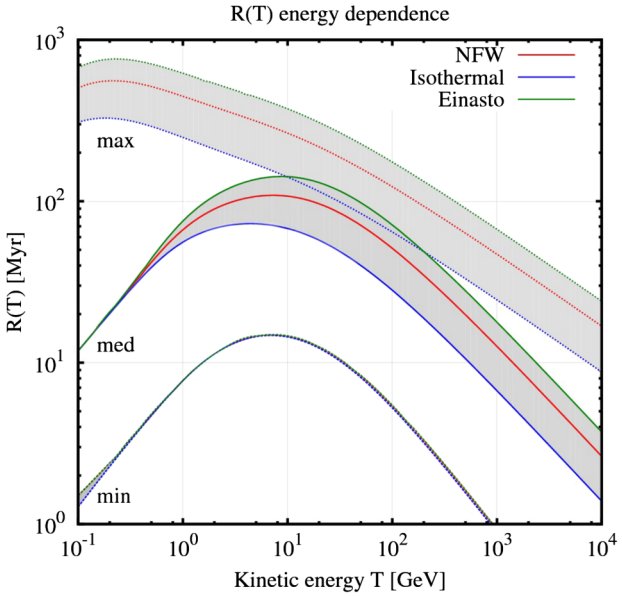

FIG. 13 (color online). The function $R(T)$, plotted for different dark matter profiles and propagation settings. The filled grey areas show the differences in $R(T)$ between the density profiles for a given propagation model. The upper lines correspond to the max model, the middle lines correspond to the med model, and the lower lines correspond to the min model.

$$\rho(r) = \frac{\rho_0}{(r/a)^{\gamma}[1 + (r/a)^{\alpha}]^{(\beta-\gamma)/\alpha}}, \tag{5}$$

or as the Einasto profile,

$$\rho_{\text{Einasto}}(r) = \rho_0 \exp\left[-\frac{2}{\alpha}\left(\left(\frac{r}{a}\right)^{\alpha} - 1\right)\right], \qquad \alpha = 0.17. \tag{6}$$

Values of the free parameters ρ_0 and a in these profiles are given for the Milky Way in Table III.

The solution to the diffusion equation Eq. (3) gives the intensity $I_{\bar{d}}$ at the position of the Earth as [19,23]

$$I_{\bar{d}}(T, \mathbf{r}_{\odot}) = B\frac{v_{\bar{d}}}{4\pi}\left(\frac{\rho_0}{M_{\text{DM}}}\right)^2 R(T)\frac{\langle\sigma v\rangle}{2}\frac{dN_{\bar{d}}}{dT}, \tag{7}$$

where B is a possible boost factor, and the astrophysics is encoded in the propagation function $R(T)$. Our results for $R(T)$ are shown in Fig. 13 and agree well with those of Kadastik *et al.* [3] (when exchanging the labels for the Einasto and Moore profiles in their figure).

Combining the propagation function $R(T)$ with the calculated energy spectra of antideuterons and accounting for solar modulations by replacing T with $T_{\odot} = T - |Ze|\phi_{\text{Fisk}}$ with $\phi_{\text{Fisk}} = 0.5$ GV [24], we are in a position to determine the intensity of antideuterons at the position of the Earth. For the final results, we adopt for the thermally averaged cross section $\langle\sigma v\rangle = 3 \times 10^{-26}$ cm^3/s, a boost factor $B = 1$ for each annihilation channel, and use the NFW density profile.

The resulting intensity of antideuterons using the med propagation parameters is shown in Fig. 14. We see that there is a significant enhancement in the peaks of the spectra going from the isotropic to the correct Monte Carlo approach. This enhancement is most significant for the 1 TeV W^+W^- case, where the peak in the Monte Carlo approach is 2 orders of magnitudes higher than in the isotropic approach.

In Fig. 15 we compare the intensities predicted by HERWIG++ and PYTHIA simulations, giving an estimate on the uncertainty in the hadronization. From the figure, we see that the uncertainty in the propagation model leads to a

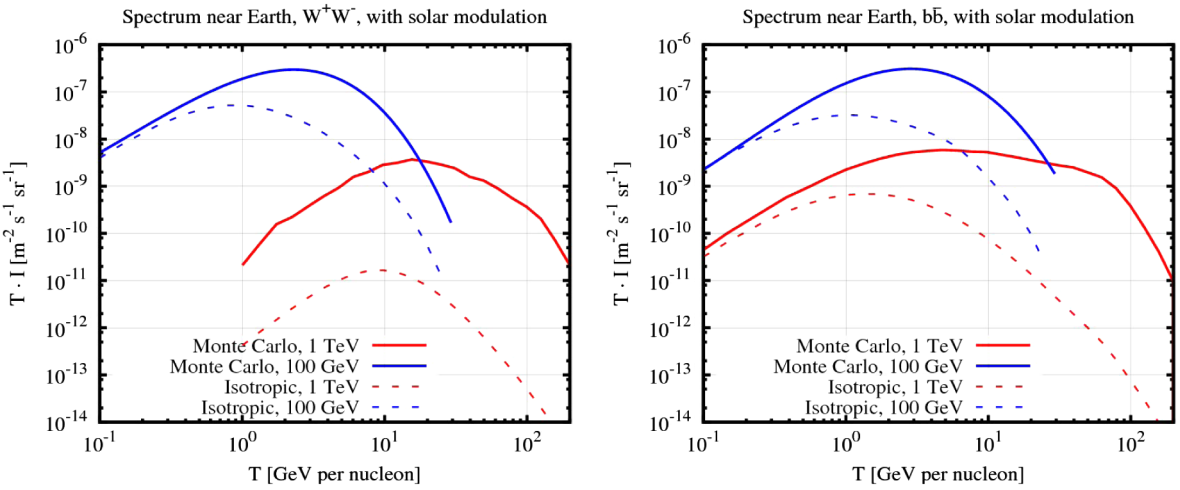

FIG. 14 (color online). Antideuteron spectra near Earth after propagation and solar modulation. Calculations are done for dark matter masses of 1 TeV and 100 GeV, using the NFW density profile and the med propagation parameters. In both plots, we assumed a thermally averaged cross section of $\langle\sigma v\rangle = 3 \times 10^{-26}$ cm^3/s. Continuous lines show the result for the Monte Carlo approach, while dashed lines show the result from the isotropic approach.

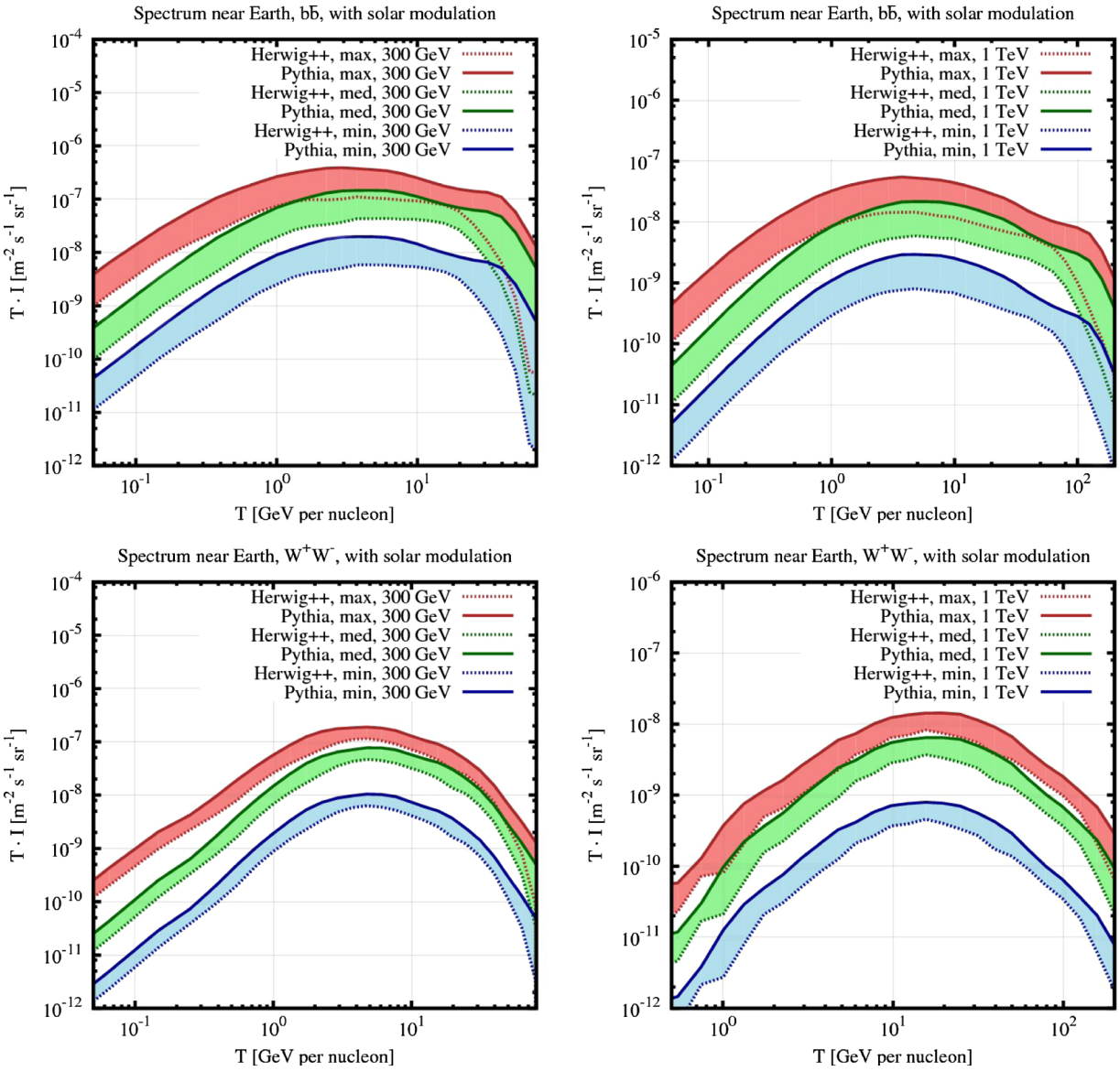

FIG. 15 (color online). Comparison of the antideuteron spectra from HERWIG++ and PYTHIA near Earth after propagation and solar modulation. The plots show the results for dark matter masses of 1 TeV and 300 GeV, using the NFW density profile and varying propagation parameters. A thermally averaged cross section of $\langle\sigma v\rangle = 3 \times 10^{-26}$ cm^3/s was assumed.

spread in the final antideuteron spectrum of $\sim$1.5 orders of magnitude, while the uncertainty in hadronization generally leads to an uncertainty of a factor 2–4, depending on the process in question. For most energies, the uncertainty in the propagation clearly dominates over the uncertainty from hadronization. For the quark channel, however, the uncertainty in hadronization becomes competitive for energies corresponding to $x > 10^{-1}$. Because of the shift in kinetic energy due to solar modulation, the sharp rise in uncertainty at low energies in the W^+W^- channel is not visible in Fig. 15, even with extended plot ranges. We expect, however, that this uncertainty will become important for relevant ranges of the spectrum for DM masses in the TeV range.

V. CONCLUSIONS

We calculated the antideuteron yield in dark matter annihilations in the coalescence model on an event-by-event basis and presented the resulting antideuteron fluxes for quark and gauge boson final states. We showed that deuteron production is very sensitive to the hadronization model employed. Comparing our results using the HERWIG++ Monte Carlo simulation to earlier results using PYTHIA, we found that the predicted antideuteron yield varies by a factor $\sim$3 for $x \lesssim 0.1$, $T \gtrsim 0.01$ GeV in the quark channel, and a factor $\sim$2 in the range $10^{-3} \lesssim x \lesssim 0.5$ in the gauge boson channel. Outside these ranges, the uncertainty increases rapidly in both

channels. Varying the parameters of the cluster hadronization model employed in HERWIG++ within the range suggested in Ref. [15] does not lead to significant additional differences in the antideuteron yield, taking into account that a recalibration of p_0 absorbs a pure change in the antideuteron multiplicity. Using the differences between HERWIG++ and PYTHIA as an estimate for the uncertainty introduced by the hadronization models, this results in an uncertainty of a factor of 2–4 on the observable intensity. While this is generally subdominant to the uncertainty from the propagation model at around 1.5 orders of magnitude, it is potentially dominant for the gauge boson channel at low energies for DM masses in the TeV range and above. We also showed the importance of $n > 2$ final states for annihilations of DM particles with masses $\gtrsim 10$ TeV.

ACKNOWLEDGMENTS

We are grateful to Sergey Ostapchenko and Are Raklev for useful discussions, and to Pat Scott for comments on the text.

[1] K. Griest and M. Kamionkowski, Phys. Rev. Lett. **64**, 615 (1990); L. Hui, Phys. Rev. Lett. **86**, 3467 (2001).
[2] F. Donato, N. Fornengo, and P. Salati, Phys. Rev. D **62**, 043003 (2000).
[3] M. Kadastik, M. Raidal, and A. Strumia, Phys. Lett. B **683**, 248 (2010).
[4] L. A. Dal, master's thesis, Norwegian University of Science and Technology, 2011 [http://urn.kb.se/resolve?urn=urn:nbn:no:ntnu:diva-12634].
[5] S. Gieseke *et al.*, arXiv:1102.1672.
[6] T. Sjostrand, S. Mrenna, and P. Z. Skands, Comput. Phys. Commun. **178**, 852 (2008).
[7] A. Schwarzschild and C. Zupancic, Phys. Rev. **129**, 854 (1963).
[8] J. I. Kapusta, Phys. Rev. C **21**, 1301 (1980).
[9] F. Donato, N. Fornengo, and D. Maurin, Phys. Rev. D **78**, 043506 (2008).
[10] C. B. Brauninger and M. Cirelli, Phys. Lett. B **678**, 20 (2009).
[11] S. Schael *et al.* (ALEPH Collaboration), Phys. Lett. B **639**, 192 (2006).
[12] B. Andersson, *The Lund Model*, Cambridge Monographs on Particle Physics, Nuclear Physics and Cosmology (Cambridge University Press, Cambridge, England, 1994).
[13] D. Amati and G. Veneziano, Phys. Lett. **83B**, 87 (1979); Y. L. Dokshitzer and S. I. Troian, Leningrad Nuclear Physics Institute, Report No. N922 (1984).
[14] R. K. Ellis, W. J. Stirling, and B. R. Webber, *QCD and Collider Physics*, Cambridge Monographs on Particle Physics, Nuclear Physics and Cosmology (Cambridge University Press, Cambridge, England, 2003).
[15] P. Richardson and D. Winn, arXiv:1207.0380.
[16] J. Alwall, M. Herquet, F. Maltoni, O. Mattelaer, and T. Stelzer, J. High Energy Phys. 06 (2011) 128.
[17] M. Cirelli, G. Corcella, A. Hektor, G. Hütsi, M. Kadastik, P. Panci, M. Raidal, F. Sala, and A. Strumia, J. Cosmol. Astropart. Phys. 03 (2011) 051.
[18] This is a factor 100 lower than the value obtained considering only Z emission from external fermion lines; cf. V. Berezinsky, M. Kachelrieß, and S. Ostapchenko, Phys. Rev. Lett. **89**, 171802 (2002).
[19] F. Donato, N. Fornengo, D. Maurin, and P. Salati, Phys. Rev. D **69**, 063501 (2004).
[20] A. Baldini, V. Flaminio, W. G. Moorhead, and D. R. O. Morrison, in *Reaction 531–599*, edited by H. Schopper, Springer-Materials—The Landolt-Börnstein Database, doi:10.1007/10367917_24.
[21] C. Amsler *et al.* (Particle Data Group Collaboration), Phys. Lett. B **667**, 1 (2008).
[22] J. F. Navarro, C. S. Frenk, and S. D. M. White, Astrophys. J. **462**, 563 (1996).
[23] D. Maurin, F. Donato, R. Taillet, and P. Salati, Astrophys. J. **555**, 585 (2001).
[24] L. J. Gleeson and W. I. Axford, Astrophys. J. **154**, 1011 (1968).